



## Islet-on-a-chip: Biomimetic micropillar-based microfluidic system for three-dimensional pancreatic islet cell culture

Patrycja Sokolowska <sup>a,b,1</sup>, Kamil Zukowski <sup>c</sup>, Justyna Janikiewicz <sup>b</sup>, Elzbieta Jastrzebska <sup>a</sup>, Agnieszka Dobrzyn <sup>b</sup>, Zbigniew Brzozka <sup>a,\*</sup>

<sup>a</sup> Medical Biotechnology, Faculty of Chemistry, Warsaw University of Technology, Poland

<sup>b</sup> Laboratory of Cell Signaling and Metabolic Disorders, Nencki Institute of Experimental Biology of Polish Academy of Sciences, Warsaw, Poland

<sup>c</sup> Centre for Advanced Materials and Technologies CEZAMAT, Warsaw University of Technology, Poland



### ARTICLE INFO

#### Keywords:

Lab-on-a-chip system  
Pancreatic islet  
Islet-on-a-chip diabetes mellitus  
Insulin secretion  
Glucagon secretion  
Microfluidic system  
Three-dimensional cellular model

### ABSTRACT

Type 2 diabetes is currently one of the most common metabolic diseases, affecting all ages worldwide. As the incidence of type 2 diabetes increases, a growing number of studies focus on islets of Langerhans. A three-dimensional research model that maps islet morphology and maintains hormonal balance *in vivo* is still needed. In this work, we present an Islet-on-a-chip system, specifically a micropillar-based microfluidic platform for three-dimensional pancreatic islet cell culture and analysis. The microfluidic system consisted of two culture chambers that were equipped with 15 circular microtraps each, which were built with seven round micropillars each. Micropillars in the structure of microtraps supported cell aggregation by limiting the growth surface and minimizing wall shear stress, thereby ensuring proper medium diffusion and optimal culture conditions for cell aggregates. Our system is compatible with microwell plate readers and confocal laser scanning microscopes. Because of optimization of the immunostaining method, the appropriate cell distribution and high viability and proliferation up to 72 h of culture were confirmed. Enzyme-linked immunosorbent assays were performed to measure insulin and glucagon secretion after stimulation with different glucose concentrations. To our knowledge, this is the first Lab-on-a-chip system which enables the formation and three-dimensional culture of cell aggregates composed of commercially available  $\alpha$  and  $\beta$  pancreatic islet cells. The specific composition and arrangement of cells in the obtained model corresponds to the arrangement of the cells in rodent pancreatic islets *in vivo*. This Islet-on-a-chip system may be utilized to test pathogenic effectors and future therapeutic agents.

### 1. Introduction

Diabetes mellitus remains the most common chronic disease globally, characterized by highly elevated blood glucose levels (hyperglycemia) that result either from defects in insulin production or an aberrant action of this hormone in insulin-sensitive tissues (Jia et al., 2019; Katsarou et al., 2017). Nearly 80% of all diabetes mellitus cases can be classified as type 2 diabetes. The onset of type 2 diabetes is driven by metabolic, environmental, and genetic factors (DeFronzo et al., 2015). For many years, scientists have been trying to study various factors that impact its development (Zheng et al., 2018). Currently, research on the treatment of diabetes is performed in several directions that combine biotechnology, engineering, transplantation, and the use of stem cells to deliver fully functional islets of Langerhans (Rodeman

and Hatipoglu, 2018; Wszola et al., 2015). These approaches are achieved by applying (1) a two-dimensional (2D) model, in the form of a cell monolayer or co-culture, (2) a three-dimensional (3D) model that consists of one or two types of cells, and (3) entire pancreatic islets that are isolated from animals or humans. However, islets that are isolated by traditional methods are not a fully functional model because of the rapid loss of cell viability and islet mass (Korbutt et al., 2004). Pancreatic islets are aggregates consisting of several cell types that are mainly located in the tail of the pancreas and responsible for the maintenance of proper blood glucose levels (St-Onge et al., 1999). The most important types for diabetes research are insulin-secreting  $\beta$ -cells and glucagon-secreting  $\alpha$ -cells (Brissova et al., 2005). The size of islets and specific arrangement of the cells depend on the species of origin (Cabrera et al., 2006). In human, pancreatic islets reach an individual size of 50–400  $\mu\text{m}$ , in which

\* Corresponding author. Medical Biotechnology, Faculty of Chemistry, Warsaw University of Technology, 3 Noakowskiego St, 00-664, Warsaw, Poland.  
E-mail address: [brzozka@ch.pw.edu.pl](mailto:brzozka@ch.pw.edu.pl) (Z. Brzozka).

<sup>1</sup> First author.

$\alpha$ - and  $\beta$ -cells occur within the entire islet volume (Steiner et al., 2010). However, because of the lack of human research models, and the problem of isolating human pancreatic islet cells, most experiments are performed in rodent models (Casasnovas et al., 2019; Komatsu et al., 2020). Islets in rodents are smaller and reach dimensions only up to 200  $\mu\text{m}$ . The  $\alpha$ -cells are located in the periphery of the islet with mantle  $\beta$ -cells (Steiner et al., 2010). Imitating islet architecture is one key to develop successful therapies, thus resembling *in vivo* conditions as much as possible.

Studies of insulin secretion are often performed with  $\beta$ -cells in 2D cultures. However, such a model is insufficient, with significant differences between hormone secretion in the 2D and 3D models (Chowdhury et al., 2013). Additionally, insulin secretion depends on signaling between different cell types. Therefore, a complete model of pancreatic islets of all cell types should be developed (Guo-Parke et al., 2012). Most existing approaches for the creation of 3D pancreatic islet cell cultures are based on self-assembly and hanging drop methods (Jia et al., 2007; Ware et al., 2016). However, in recent years, the use of Lab-on-a-chip systems for the culture and analysis of 3D structures under appropriate flow conditions has become promising. (Yeo et al., 2011). In contrast to the above-mentioned method, the culture of 3D structures in Lab-on-a-chip systems has many advantages, such as mapping *in vivo* conditions, no need to transfer aggregates (e.g. to multi-well plates for analysis), and the possibility to perform culture and analysis in one device. In such a way, the risk of damage and disorganization of the created structures is minimized. To date, microfluidic systems have been successfully used to create such models as Lung-on-a-chip (Huh et al., 2010), Kidney-on-a-chip (Weber et al., 2018), Heart-on-a-chip (Ahn et al., 2018), and Liver-on-a-chip (Hassan et al., 2020), and used for studying intracellular islet signaling and hormone secretion (Castiello et al., 2016).

To develop a 3D model, the proper geometry of the system needs to be designed, and appropriate materials need to be selected for promoting the formation of cell aggregates that mimic islet architecture. The use of microwells is the most popular solution to obtain 3D aggregates and culture isolated islets in microfluidic systems (Jun et al., 2019). In such a structure, the introduced cells fall to the bottom of a hydrophobic well and create a 3D structure (Hirano et al., 2017). Nevertheless, microfluidic systems face problems concerning the random organization of cells and lack of control over the size of aggregates. This may result in a necrotic core in the islet, lower viability, and a lower degree of cell proliferation. Microfluidic systems can significantly support the creation of 3D structures and reduce the time that is necessary to create them. Here, we present a 3D cellular model of pancreatic islets that was developed using a micropillar-based microfluidic system. This 3D model consists of two major types of cells that form the pancreatic islet: glucagon-secreting  $\alpha$ -cells and insulin-secreting  $\beta$ -cells. Our microfluidic system enables the formation, culture, and the microscopic observation of aggregates (pseudoislets). Further, our microfluidic system also allows for the analysis of secreted insulin and glucagon. In this system, we obtained 3D cell aggregates with dimensions of 165–185  $\mu\text{m}$ . The aggregate architecture corresponded to rodent pancreatic islets, which was confirmed by immunofluorescence staining. The functionality of the model was confirmed by insulin and glucagon secretion studies that were based on enzyme-linked immunosorbent assays (ELISAs). To our knowledge, this is the first report of the development of a 3D model of the co-culture of INS-1E and  $\alpha$ -TC1-6 cells, which closely resembled *in vivo* conditions.

## 2. Materials and methods

### 2.1. Microfluidic system

The microfluidic system that was used in this study consisted of two PDMS layers: a bottom layer with a microstructures and a top layer without microstructures (used as a cover layer). For confocal

microscopy, the top layer was replaced with a borosilicate coverslips (24 mm length, 60 mm width, and 170  $\mu\text{m}$  thickness). The bottom layer was obtained in a few steps. (see Supplementary Materials). Afterward, the microchannel structure was replicated in PDMS (Sylgard 184, Dow Corning) using replica molding techniques (see Supplementary Materials).

The microfluidic system consisted of two identical microstructures (one for the test sample and one for the control) that were arranged in parallel. Each microstructure contained one microchannel (8000  $\mu\text{m}$  length, 200  $\mu\text{m}$  width, 200  $\mu\text{m}$  height) that was equipped with one inlet and one outlet. Each of the microchannels was connected with an elliptical microchamber (9000  $\mu\text{m}$  length, 6000  $\mu\text{m}$  width, 200  $\mu\text{m}$  height), which were equipped with 15 circular microtraps (280  $\mu\text{m}$  diameter, 200  $\mu\text{m}$  height) that were built with seven round micropillars each (145  $\mu\text{m}$  length, 145 width, 200  $\mu\text{m}$  height). The micropillars were arranged at 20  $\mu\text{m}$  intervals in a semicircle with a wide open 160  $\mu\text{m}$  inlet space in the direction of cell introduction. Culture microchambers were arranged in accordance with the culture wells on a standard Sarstedt 5022411 multiwell plate. To determine the proper cell culture conditions that prevailed in this microfluidic system, the visualization and simulation of particle tracking and wall shear stress using the Microelectromechanical Systems (MEMS) simulation module of COMSOL Multiphysics software were performed.

### 2.2. Three-dimensional pseudoislet cell cultures in the microfluidic systems

Two cell lines were used in the experiments. Mouse pancreatic islet  $\alpha$ -cells ( $\alpha$ -TC1-6) were purchased from the American Type Culture Collection (catalog no. CRL-2934). The rat INS-1E insulinoma  $\beta$ -cell line was a gift from Dr. Pierre Maechler (University of Geneva, Geneva, Switzerland). The specific composition of the culture media is described in the Supplementary materials. In each of the microfluidic systems, the culture was performed according to the following protocol. Before starting a new experiment, the microfluidic systems were sterilized for 30 min using ultraviolet light (Black Ray, model B100AP), and 70% ethanol (PoCh, catalog no.396420113) which was introduced through the inlet of the microchannel. After the sterilization step, a mixture of INS-1E and  $\alpha$ -TC1-6 culture medium (prepared in a 1:1 ratio) was introduced into the microfluidic system at a flow rate of 10  $\mu\text{l}/\text{min}$  over 10 min. The microfluidic system was then placed in an incubator (5% CO<sub>2</sub>, 37 °C, HERA-cell 150 incubator, ThermoScientific) for the next 2 h. Finally, an  $\alpha$ -TC1-6 cell suspension ( $2 \times 10^6$  cells/ml) and INS-1E cell suspension ( $2 \times 10^6$  cells/ml) were prepared by trypsinization (0.25% Trypsin, Sigma-Aldrich) and mixed in a 1:2 ratio. This cell suspension was introduced into the microfluidic system through the inlet of the microchannel at a flow rate of 15  $\mu\text{l}/\text{min}$  over 1 min. To remove cells that were not placed in the microtraps, the mixture of INS-1E and  $\alpha$ -TC1-6 culture media (1:1 ratio) was introduced into the microfluidic system at a flow rate of 10  $\mu\text{l}/\text{min}$  over 5 min. The microfluidic systems with the introduced cells were placed in an incubator for the next 24 h to create cell aggregates (pseudoislets). After 24, 48, and 72 h, the culture medium was exchanged at a flow rate of 10  $\mu\text{l}/\text{min}$ . The peristaltic pumps (Ismatec Reglo-Digital MS-4/12) were used for introduction of all fluids and cells at each stage of the experiment.

### 2.3. Proliferation and viability of cells in pseudoislets

To assess cell proliferation, islet aggregates were incubated with a 10% vol AlamarBlue solution (Abcam, catalog no. ab176748). The AlamarBlue solution was prepared in culture medium (mixture of INS-1E and  $\alpha$ -TC1-6 culture media in a 1:1 ratio) and introduced into the microfluidic system at a flow rate of 10  $\mu\text{l}/\text{min}$  over 3 min. The microfluidic system was then incubated in an incubator (37 °C, 5% CO<sub>2</sub>) for 50 min. Because of the design of the microfluidic chambers in accordance with the culture wells on a standard multiwell plate, proliferation

measurements were performed in a multiwell plate reader (Tecan Infinite 200 Pro). The fluorescence intensity was measured at an excitation wavelength of 552 nm and emission wavelength of 583 nm.

To determine cell viability, a test with propidium iodide (PI; Sigma Aldrich, catalog no. P4864) and calcein-AM (CAM; Sigma Aldrich, catalog no. C1359) was performed each day up to 72 h of culture. A solution of PI and CAM was prepared according to the following procedure: 1  $\mu$ l of CAM (2 mM) and 1  $\mu$ l of PI (1 mg/ml) were added to a

0.5 ml mixture of INS-1E and  $\alpha$ -TC1-6 culture media (1:1 ratio). This solution was introduced into the microfluidic system for 3 min at a flow rate of 10  $\mu$ l/min. The microchip with the introduced dyes was incubated at 37 °C with 5% CO<sub>2</sub> for 20 min. Afterward, the cell aggregates were observed using a fluorescence microscope (Olympus IX71). The CAM fluorescence intensity was measured at an excitation wavelength of 490 nm and emission wavelength of 515 nm. The PI fluorescence intensity was measured at an excitation wavelength of 535 nm and

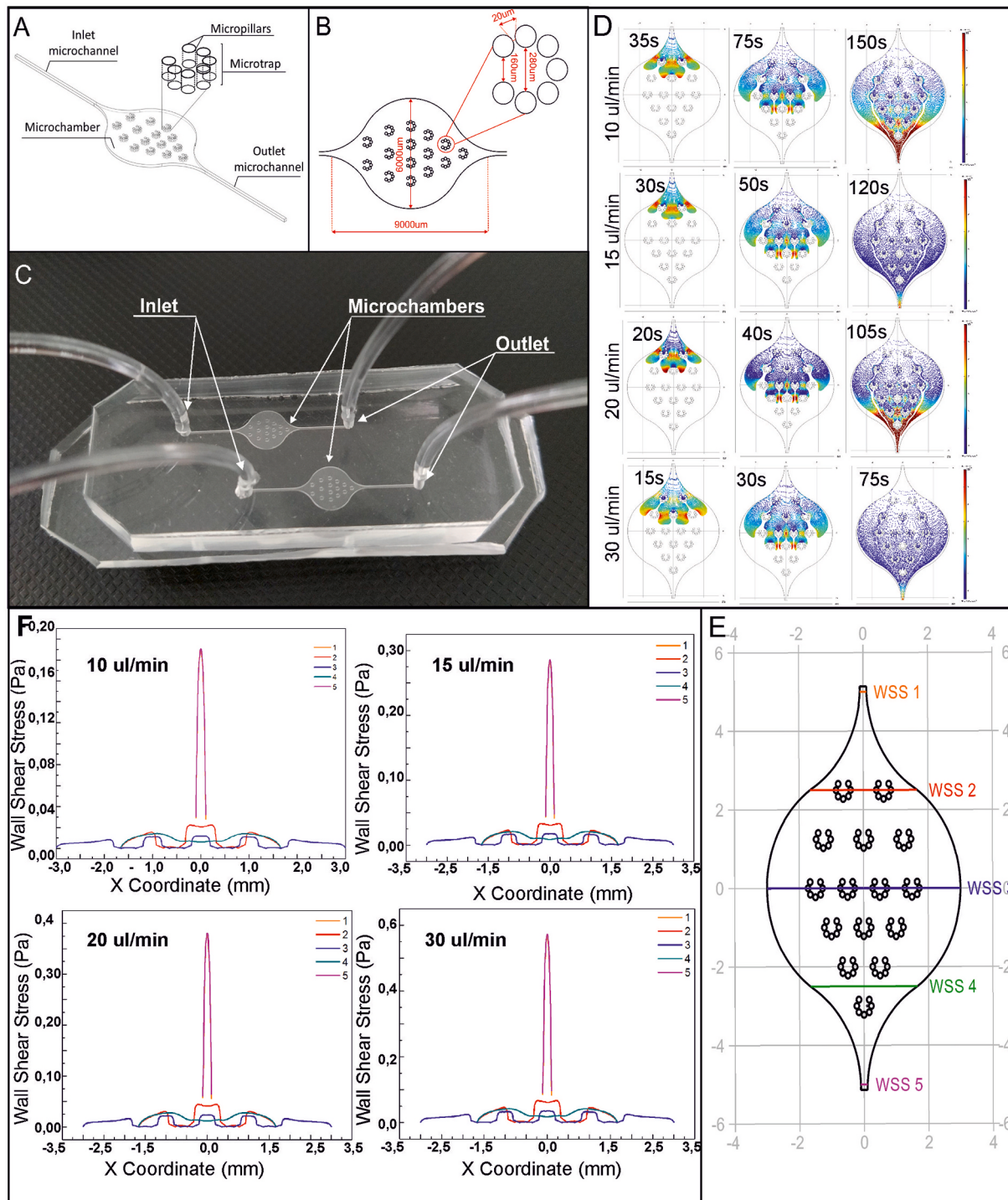


**Fig. 1.** A, B. Geometry of one microchamber of the microfluidic system for the aggregation and culture of  $\alpha$ -TC1-6 and INS-1E cells. C. PDMS/PDMS microfluidic system. D. Results of COMSOL Multiphysics simulation for micropillar-based microfluidic system geometry. Cell suspension flow modeling in microchambers for cells at a density of  $2 \times 10^6$  cell/ml and different flow rates (10, 15, 20, and 30  $\mu$ l/min). E. Different regions of the microchamber where wall shear stress simulations were performed. F. Line graph of wall shear stress distribution.

emission wavelength of 617 nm. The number of dead and live cells were determined by fluorescence intensity profile analysis using cellSens Dimension image analysis software (Olympus).

#### 2.4. Immunofluorescence staining

To confirm the morphology and appropriate participation of  $\alpha$ - and  $\beta$ -cells in the obtained pseudoislets, the method of immunofluorescence staining using antibodies was optimized.

All of the reagents were introduced into the micropillar-based microfluidic systems through the microchannel inlet at a flow rate of 10  $\mu$ l/min. A two-step procedure with primary and secondary antibodies (See supplementary materials) was used. Observations of stained pseudoislets that were composed of  $\alpha$ - and  $\beta$ -cells in the 2D and 3D (scanning and analysis of the entire aggregate was performed along the Z axis, layer by layer) views were performed using a Fluoview FV10i confocal microscope (Olympus). Image analysis was performed using Olympus Fluoview Fv10i software.

#### 2.5. Quantitative determination of insulin and glucagon secretion

To confirm functionality of the  $\alpha$ - and  $\beta$ -cells aggregates, insulin and glucagon secretion tests were performed 24 h after introducing the cells into the microfluidic system. The test was performed after stimulating the aggregates with low (2.75 mM) and high (16.5 mM) glucose concentrations, respectively. (See supplementary materials). The obtained samples were stored at  $-20^{\circ}\text{C}$  until ELISA was performed. The tests were performed in three independent replicates (three micropillar-based microfluidic systems). Insulin and glucagon secretion from pseudoislets was confirmed after their stimulation with glucose using the Rat/Mouse Insulin ELISA Kit (Millipore, catalog no. EZRMI-13K) and Glucagon Chemiluminescent ELISA Kit (Millipore, catalog no. EZGLU-30K) according to the manufacturer's instructions. Absorbance (450 nm and 590 nm) and luminescence ( $\sim$ 425 nm) were read in a multiwell plate reader (Tecan Infinite 200 Pro).

#### 2.6. Statistical analysis

All of the quantitative data are expressed as mean  $\pm$  standard deviation (SD), based on at least three independent experiments. The statistical analysis was performed using one-way analysis of variance (ANOVA). Values of  $p < 0.05$  were considered statistically significant.

### 3. Results and discussion

#### 3.1. Microfluidic system

The designed microfluidic system consisted of two PDMS layers with microstructures (Fig. 1C). The geometry of the microfluidic system consisted of two identical, parallel, independent culture microchambers that were equipped with 15 microtraps each. Because of this arrangement, we could obtain 15 spherical cell aggregates and subsequently analyze them in two replications. The typical size of mammalian pancreatic islets ranges from 100 to 200  $\mu\text{m}$  (Steiner et al., 2010). The geometry of the microfluidic system consisted of a culture chamber with 15 round microtraps ( $280 \mu\text{m} \times 280 \mu\text{m}$ ) with seven micropillars each ( $145 \mu\text{m} \times 145 \mu\text{m} \times 200 \mu\text{m}$ ). Such dimensions of the microtraps ensured the formation of aggregates with a diameter of  $\sim$ 185  $\mu\text{m}$ . Due to the use of thin glass in the construction of the culture microchambers arranged in accordance with the culture wells on a standard Sarstedt 5022411 multiwell plate the proposed microfluidic system has been successfully used to study the obtained structures using fluorescence microscopy, confocal microscopy and multi-well plate readings. To predict the distribution of cells in the microtraps and culture chambers, and the flow distribution of all introduced solutions, a computer simulation using the MEMS simulation module of COMSOL Multiphysics

software was performed. The simulation (particle tracing and wall shear stress) was performed for cells at a density of  $2 \times 10^6$  cell/ml and with different flow rates (10, 15, 20 and 30  $\mu\text{l}/\text{min}$ ). In the micropillar-based microfluidic system for each flow rate, the flow distribution of the cell suspension was steady, and the cells were delivered to each of the microtraps (Fig. 1D). Wall shear stress that was generated in the microchamber directly depended on the area of the microchamber, the presence of microtraps, and the flow rate (Fig. 1F). The highest wall shear stress occurred for the areas at the inlet and outlet of the microchamber. The lowest wall shear stress occurred in the center of the microtraps and was 20 times lower than in the outlet and inlet. Higher wall shear stress occurred in the microchamber in the area between the microtraps that were spaced at longer distances from each other. The most equitable distribution of wall shear stress occurred in the center of the chamber (see WSS 3 in Fig. 1E). The highest shear stress in the chamber between the microtraps was observed at the highest flow rate (30  $\mu\text{l}/\text{min}$ ; i.e., a threefold increase compared with 10  $\mu\text{l}/\text{min}$ ). However, for each of the analyzed flow rates, wall shear stress inside the microtraps was close to 0. Thus, a flow rate of 15  $\mu\text{l}/\text{min}$  was chosen for cell introduction, and a flow rate of 10  $\mu\text{l}/\text{min}$  was chosen to deliver the other solutions.

The proper distribution of cells in each of the microtraps was confirmed with a density of  $2 \times 10^6$  cell/ml and a cell suspension loading rate of 15  $\mu\text{l}/\text{min}$  (these conditions were confirmed experimentally). The microtraps in the geometry of the micropillar-based microfluidic system allowed for the minimization of wall shear stress and ensured proper medium diffusion and optimal culture conditions for cell aggregates.

#### 3.2. Three-dimensional islet cell aggregates in the micropillar-based microfluidic system

Under physiological conditions,  $\alpha$ -cells constitute  $\sim$ 25% and  $\beta$ -cells constitute  $\sim$ 60% of all cells in the islet (approximately 1:2 ratio) (Röder et al., 2016; Steiner et al., 2010). To mimic *in vivo* conditions, the key step was to select an appropriate microfluidic system geometry and an appropriate  $\alpha$ - and  $\beta$ -cell ratio. Immediately after introducing the cell suspension (in  $\alpha$  to  $\beta$ -cells ratio 1:2) into the microchip, each of the 15 microtraps was filled with a cell suspension that formed clusters of cells (0 h; Fig. 2). At this point, the cells were washed with fresh medium. Cells that were outside the microtraps were washed from the microfluidic system. After 24 h of incubation (5%  $\text{CO}_2$ ,  $37^{\circ}\text{C}$ ), the cells in each of the 15 microtraps formed spherical aggregates with a dimension of 165–185  $\mu\text{m}$ . The aggregates were then successfully cultured for the next 72 h. Fresh medium was introduced daily. The aggregation of pancreatic islet cells in the literature was mostly achieved after  $\sim$ 48 h, and the process of islet formation sometimes lasted up to 6 days (Hirano et al., 2017b; Lee et al., 2018). Because of the limited growth surface through the hydrophobic material and micropillar structure in the microchip geometry, the complete aggregation and formation of pseudoislets were achieved 24 h after introducing the cells into the system.

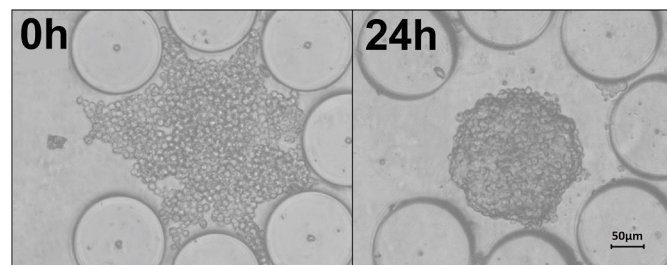


Fig. 2. Co-cultures of  $\alpha$ - and  $\beta$ -cells immediately (0 h) (left) and 24 h (right) after introducing the cells into the microfluidic system. The diameter of each pseudoislet ( $n = 15$ ) was  $\sim$ 175  $\mu\text{m} \pm 10 \mu\text{m}$ .

### 3.3. Proliferation and viability of pancreatic cell aggregates

Proliferation and viability tests were conducted to evaluate the impact of the selected conditions in the microfluidic system (i.e., flow rate, incubation time, and appropriate cell density) on the degree of culture viability. Viability and proliferation were assessed daily throughout the entire time of culture (from 24 to 72 h of culture). A high viability of the obtained aggregates was observed on each day of culture (Fig. 3A). Cell viability on the last day of culture (72 h) decreased to ~80% compared with the first day (24 h). Furthermore, no necrotic core was observed in the obtained aggregates. The degree of proliferation compared with the first day of culture (24 h) increased to 1.1 and 1.2 after 48 and 72 h, respectively (Fig. 3B). The gaps between the micropillars ensured constant diffusion of the culture medium and other factors inside the aggregates. The geometry of the microtraps also minimized shear stress and prevented fragmentation and the washing out of the aggregates from the microfluidic system. In summary, the parameters that were applied for the cell cultures did not have a toxic effect on the 3D structures of pancreatic islets.

### 3.4. Study of pancreatic islet aggregate structures and composition

Rodent pancreatic islets are well-defined structures with a specific composition and location of cells.  $\alpha$ -cells are arranged on the periphery of the islet and  $\beta$ -cells are arranged in the islet core. The main goal of the present study was to develop a microfluidic system that mimics native pancreatic islet structure. In order to confirm that the cell aggregates have the proper architecture and that the cells are distributed appropriately within the microfluidic system, the method of immunofluorescence staining and analysis was performed using a laser scanning

confocal microscope. Thanks to the combination of precise labeling (with antibodies) of  $\alpha$ - and  $\beta$ -cells and scanning the structure across the entire volume (along the Z axis, layer by layer) of the formed pseudoislet, we were able to carefully determine the location of both types of cells. Three-dimensional structures that were obtained with culturing  $\alpha$ -TC1-6 and INS-1E cells in a 1:2 ratio in the micropillar-based microfluidic system had the same architecture (in terms of size, morphology and  $\alpha$ - and  $\beta$ -cells arrangement) as native rodent pancreatic islets. The obtained structure was spherical and well organized,  $\beta$ -cells constituted the core of the islets, whereas  $\alpha$ -cells were distributed peripherally (Fig. 4). Fluorescence intensity analysis was also performed to identify the distribution of cells in the aggregate. High insulin fluorescence intensity (green) was observed inside the aggregate, and high glucagon fluorescence intensity (red) was observed on the outer part of the aggregate (Fig. 4C), thus confirming the correct distribution of cells in the developed model.

### 3.5. Microwell-based microfluidic system vs. micropillar-based microfluidic system

The cell culture in the developed micropillar-based microfluidic system was compared with a microwell-based microfluidic system (which is most often used in the study of cell spheroids). Microfluidic system with microwell-based geometry was previously used to create and culture cancer (A549) and non-malignant (MRC-5) cell spheroids. The geometry of this system consisted of a network of microchambers (2700  $\mu\text{m}$  diameter, 100  $\mu\text{m}$  depth). The network of microstructures consisted of three rows, each with four microchambers. Each microchamber contained seven U-shaped culture microwells (500  $\mu\text{m} \times 500 \mu\text{m}$ ) (Zuchowska et al., 2017).

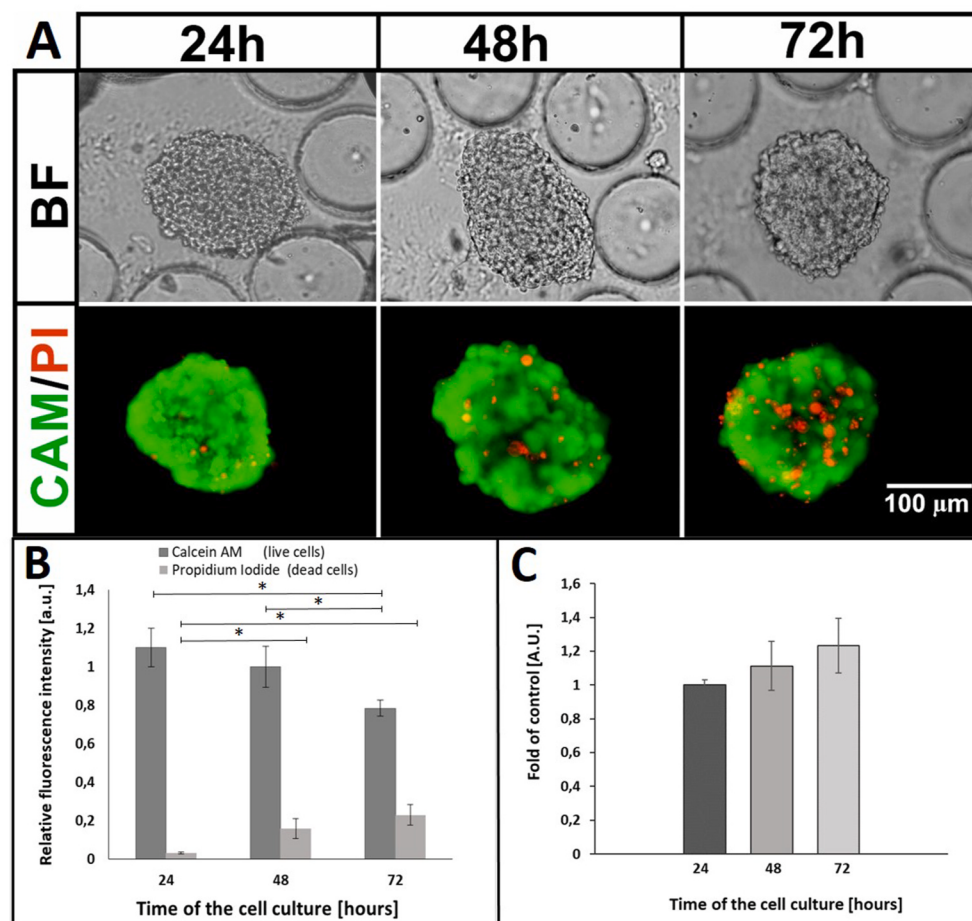


**Fig. 3.** A. Co-culture of  $\alpha$ - and  $\beta$ -cells after 24, 48, and 72 h of culture in the micropillar-based microfluidic system (bright field [BF]). Differential staining of  $\alpha$ - and  $\beta$ -cell co-culture with calcein-AM (CAM; live cells) (green) and propidium iodide (PI; dead cells) (red). B. Relative values of fluorescence intensity on the following days of cell culture at 24, 48, and 72 h n = 3. C. Co-culture proliferation after 24, 48, and 72 h of culture in the designed micropillar-based microfluidic system. n = 3. \*p < 0.05. (For interpretation of the references to color in this figure legend, the reader is referred to the Web version of this article.)

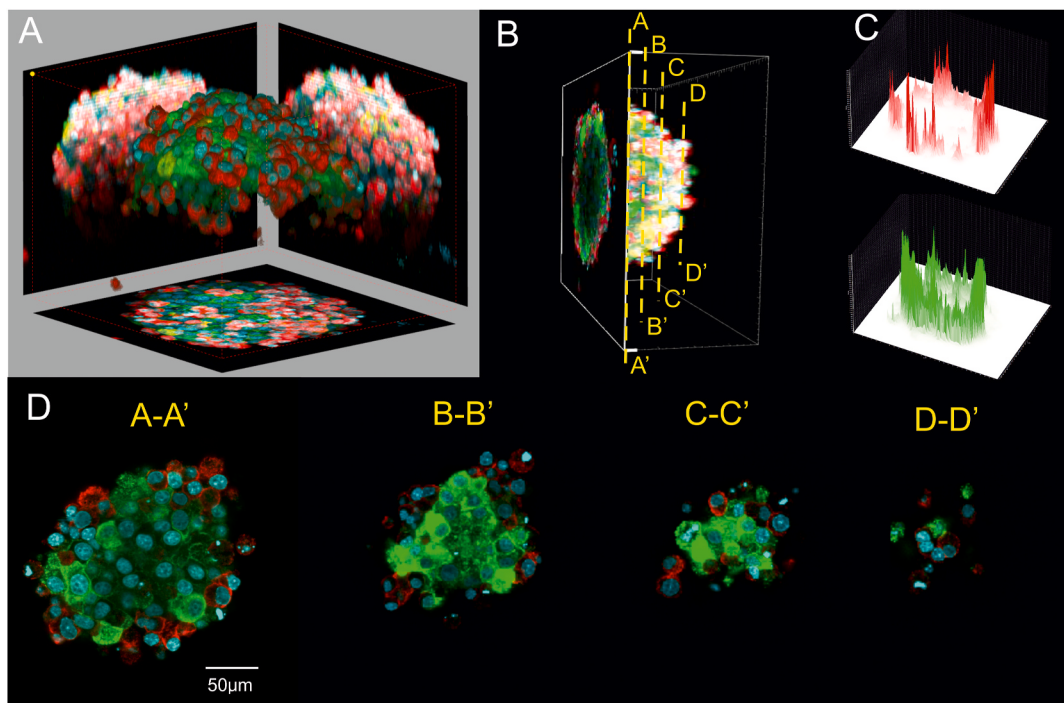


**Fig. 4.** Confirmation of the localization of  $\alpha$ - and  $\beta$ -cells by staining glucagon (conjugated with Alexa Fluor 594) (red cells) and insulin (conjugated with Alexa Fluor 488) (green cells). The cell nucleus is shown in blue (Hoechst staining). A. Three-dimensional confocal image of the obtained aggregate. B. A confocal microscope photo of a pseudoislet with cross-sectional planes. C. Fluorescence intensity at individual locations of the aggregate ( $\beta$ -cells in the core,  $\alpha$ -cells in the periphery). D. Photograph of spatial distribution of  $\alpha$ - and  $\beta$ -cells from several selected layers of the same pseudoislets. (For interpretation of the references to color in this figure legend, the reader is referred to the Web version of this article.)

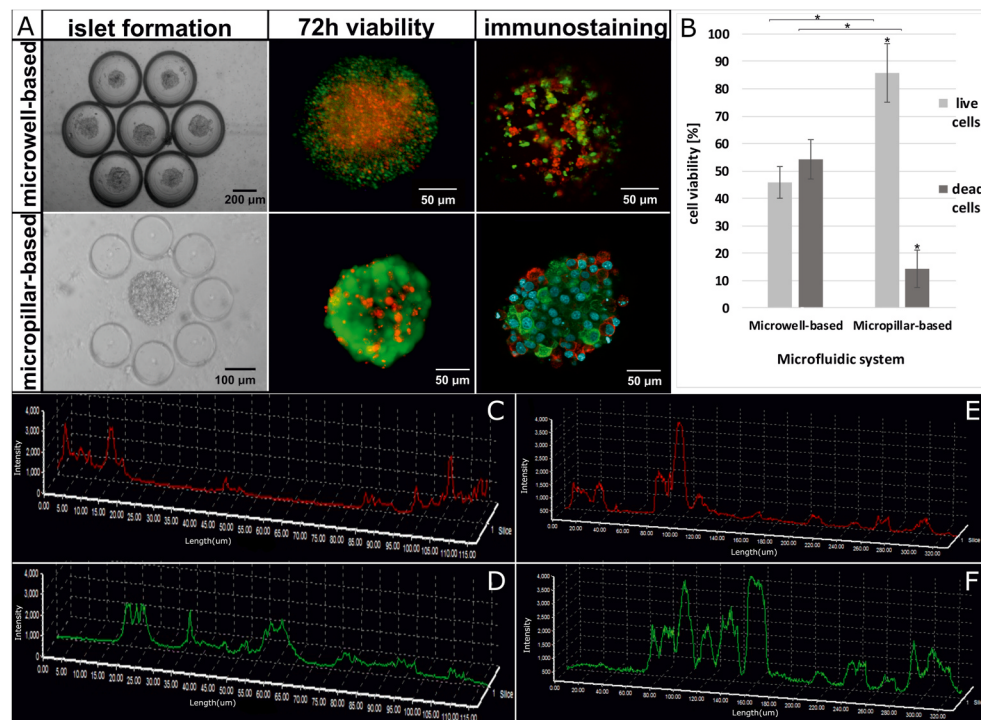


**Fig. 5.** Comparison of pancreatic islet cell culture in the microwell-based and the micropillar-based microfluidic systems. A. From the top: islet formation after 24 h of culture. Next, cell viability after 72 h of culture. Differential staining of  $\alpha$ - and  $\beta$ -cells co-culture with CAM (Calcein AM – green color – live cells) and PI (Propidium Iodide – red color – dead cells). Immunostaining – Confirmation of the localization of  $\alpha$ - and  $\beta$ -cells – staining of glucagon (conjugated with Alexa Fluor 594 – red cells) and insulin (conjugated with Alexa Fluor 488 – green cells), the cell nucleus is shown in blue (Hoechst staining). n = 3. B. Comparison of the viability of cell cultures in a microwell-based and micropillar-based microfluidic system. n = 3. \*p < 0.05 C. Analysis of the glucagon expression level obtained for a cross-section of a pseudoislet cultured in a micropillar-based microfluidic system. D. Analysis of the insulin expression level obtained for a cross-section of a pseudoislet cultured in a micropillar-based microfluidic system. E. Analysis of the glucagon expression level obtained for a cross-section of a pseudoislet cultured in a microwell-based microfluidic system. F. Analysis of the insulin expression level obtained for a cross-section of a pseudoislet cultured in a microwell-based microfluidic system. (For interpretation of the references to color in this figure legend, the reader is referred to the Web version of this article.)

referred to the Web version of this article.)

In this step of the research, a comparative cell aggregation test, cell viability assay and immunostaining were performed in the microwell-based and micropillar-based microfluidic systems. Our goal was to determine whether the microwell-based structure that is usually applied for spheroid formation can be used as a platform to create fully functional pancreatic islets. The process for cell aggregate formation from INS-1E and  $\alpha$ -TC1-6 cells was performed to completion (Fig. 5). Twenty-four hours after introducing the cells, they formed spherical aggregates in both systems (microwell-based and micropillar-based). In the microwell-based microfluidic system, the formation of spherical aggregates with dimensions of 190–230  $\mu\text{m}$  was observed in each of the seven wells. Similarly, the formation of spherical aggregates with dimensions of 165–185  $\mu\text{m}$  was noticed in each of the 15 microtraps in the micropillar-based microfluidic system. Next, viability tests using PI and CAM were performed daily (after 24, 48, and 72 h of culture). After 72 h of cell aggregates culture, the cell viability was 45.83% for cells cultured in microwell-based compared to 85.66% for cells cultured in the micropillar-based microfluidic system. Additionally, for aggregates obtained in the microwell-based microfluidic system, the necrotic core was observed after 48 h of culture and after 72 h of culture, most of the cells were dead. Contrary to this, for pseudoislets that were cultured in the micropillar-based microfluidic system, the necrotic core was not observed, and a high degree of viability was found up to 72 h of culture. Such a difference may be related to differences in medium diffusion into the aggregate inside these two geometries of the microchambers. Additionally, the cells density that is suitable for culture in the micropillar-based microfluidic system may be too high for cell culture in the microwell-based system. This can result in excessively dense packing of cells, which may result in problems with nutrient diffusion into the aggregate. Finally, cell location and cellular composition of the obtained aggregates were studied. Spherical aggregates, in which  $\beta$ -cells were located in the core and  $\alpha$ -cells were located in the periphery, were obtained only in the micropillar-based microfluidic system. In the microwell-based microfluidic system the arrangement of the cells was random, both  $\alpha$ - and  $\beta$ -cells were localized in the entire volume of the obtained aggregate. Moreover, the spherical structure of the aggregate in the microwell-based microfluidic system was disturbed. In order to confirm the distribution of the  $\alpha$ -cells and  $\beta$ -cells analysis of insulin and glucagon expression levels was performed. The graphs (Fig. 5C, D, E, F) show the distribution of the fluorescence intensity for insulin and glucagon within the cross section (middle layer: 100  $\mu\text{m}$  depth) cell aggregates for both micropillar-based and microwell-based microfluidic systems. It is clearly visible that the micropillar-based microfluidic system shows that the fluorescence intensity obtained for  $\beta$ -cells (red line) was recorded only for the cells of the internal pseudoislet layer, while the fluorescence intensity obtained for  $\alpha$ -cells (green line) was higher for the middle aggregate layer. The opposite effect was observed after analysis of cell aggregates cultured in the microwell-based

microfluidic system - both the insulin signal (green line) and glucagon (red line) were observed in the entire volume of the cell aggregate.

### 3.6. Quantitative determination of insulin secretion

The functionality of pancreatic islets is determined by assessing their insulin and glucagon secretory capacity in response to glucose stimulation (Kahn et al., 2014). When a solution with a high glucose concentration is delivered into the pancreatic islet, insulin secretion reaches a high level while the level of secreted glucagon is low. However, in the case of glucose deficiency, insulin levels should be low with simultaneously high glucagon secretion (Henquin et al., 2006; Komatsu et al., 2013; Liu et al., 2019). One of the most commonly used method of assessing the degree of hormone secretion from pancreatic islets is the ELISA (Chen et al., 2017). In this part of the present study, ELISAs of insulin and glucagon secretion in the presence of different glucose concentrations were performed. Based on the design of the two microchambers of the micropillar-based microfluidic system, stimulation of the cells with high (16.5 mM) and low (2.75 mM) glucose solutions were performed simultaneously under the same environmental conditions (Fig. 6). The level of insulin secretion in the micropillar-based microfluidic system was 1.38 ng per pseudoislet after low glucose stimulation. For high glucose, we detected 2.75 ng insulin per aggregate. For the level of glucagon secretion, an inverse relationship was observed, 0.47 and 0.21 ng glucagon per pseudoislet were secreted under low- and high-glucose conditions, respectively. These results confirmed that aggregates of INS-1E and  $\alpha$ -TC1-6 cells that were cultured in the micropillar-based microfluidic system were fully functional.

## 4. Conclusions

The present study sought to develop a fully functional model of pancreatic islets that can be used in future studies to evaluate the influence of diabetes effectors and test novel therapeutic agents. Another goal was to create a universal model of the islet that is sufficiently potent to reduce the number of animals that are necessary for such research (Sokolowska et al., 2020). To date, most research has been performed using 2D models or 3D isolated rodent islets, which rapidly lose their function in static cultures. Differences exist between measurements of insulin secretion from isolated islets in static cultures and under flow conditions (Gylfe, 2016; Rodriguez-Diaz et al., 2018). Currently, most of developed microfluidic systems with microwell geometry have been used in studies of pancreatic islets (Essaouiba et al., 2020; Kim et al., 2013) to culture freshly isolated rodent pancreatic islets or the differentiation of iPSCs toward islets of Langerhans (Jun et al., 2019a; Mohammed et al., 2009). Contrary to this, we would like to underline that thanks to the development of the proper geometry and conditions in the microfluidic system we can mimic the rodent pancreatic islet

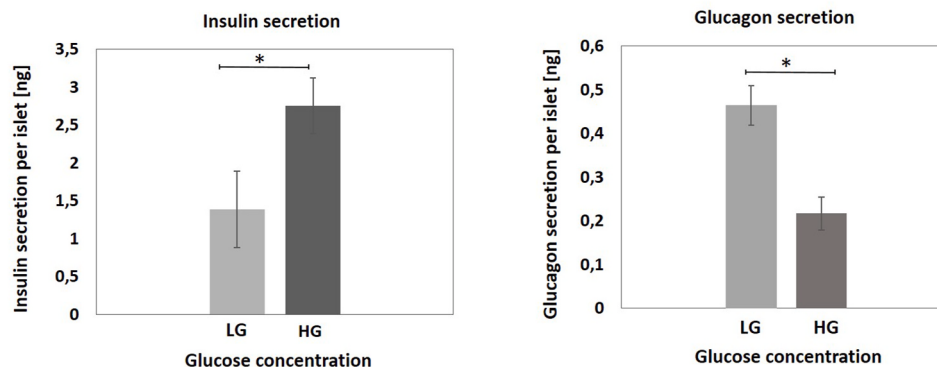


**Fig. 6.** Degree of insulin (left) and glucagon (right) secretion after stimulation with low glucose (LG; 2.75 mM) solution and a high glucose (HG; 16.5 mM) solution.  $n \geq 3$ . \* $p < 0.05$ .

without the use of living organisms. In our research, we omitted the time-consuming stage of the pancreatic islets isolation and were able to perform the entire analysis on one microfluidic device.

In the present study, a pseudoislet model that consisted of two types of cells that maintained viability, proliferation capacity, and functionality up to 72 h of culture was developed. Moreover, to further demonstrate the advantage of our model over other available systems, we compared  $\alpha$ -TC1-6 and INS-1E cell aggregation in microwell-based and micropillar-based microfluidics geometries. However, we found that pseudoislets with a high degree of viability, proliferation, and the proper arrangement of cells were obtained only in our designed micropillar-based microfluidic system. Moreover, The ELISA analysis of insulin and glucagon secretion in the designed micropillar-based microfluidic system demonstrated a proper level of hormone secretion after stimulating the pseudoislets with high and low glucose concentrations. The proposed micropillar-based microfluidic system may allow us to gain greater knowledge of hormone secretion, cell-cell communication, and causes of diabetes mellitus and develop better treatments. To our knowledge, this is the first microfluidic system in which fully functional spherical aggregates form in co-cultures of pancreatic  $\alpha$ - and  $\beta$ -cells. These aggregates correspond with the composition and localization of the cells to the rodent pancreatic islets *in vivo*.

#### CRediT authorship contribution statement

**Patrycja Sokolowska:** Conceptualization, Methodology, Formal analysis, Investigation, Writing – original draft, Visualization, Funding acquisition. **Kamil Zukowski:** Methodology, Performing computer simulations using the MEMS simulation module of the COMSOL Multiphysics software and prepare microfluidic system stamp. **Justyna Janikiewicz:** Conceptualization, Writing – review & editing. **Elzbieta Jastrzebska:** Writing – review & editing. **Agnieszka Dobrzyn:** Resources, Writing – review & editing. **Zbigniew Brzozka:** Resources, Supervision, Writing – review & editing.

#### Declaration of competing interest

The authors declare that they have no known competing financial interests or personal relationships that could have appeared to influence the work reported in this paper.

#### Acknowledgements

This work was financially supported by National Science Centre within the framework of the PRELUDIUM program (no. UMO-2019/33/N/ST4/02416). The project was implemented under the Operational Program Knowledge Education Development (2014–2020), co-financed by the European Social Fund.

#### Appendix A. Supplementary data

Supplementary data to this article can be found online at <https://doi.org/10.1016/j.bios.2021.113215>.

#### References

- Ahn, S., Ardoña, H.A.M., Lind, J.U., Eweje, F., Kim, S.L., Gonzalez, G.M., Liu, Q., Zimmerman, J.F., Pyrgiotakis, G., Zhang, Z., Beltran-Huarac, J., Carpinone, P., Moudgil, B.M., Demokritou, P., Parker, K.K., 2018. *Anal. Bioanal. Chem.* 410 (24), 6141–6154.
- Brissova, M., Fowler, M.J., Nicholson, W.E., Chu, A., Hirshberg, B., Harlan, D.M., Powers, A.C., 2005. *J. Histochem. Cytochem.* 53 (9), 1087–1097.
- Cabrera, O., Berman, D.M., Kenyon, N.S., Ricordi, C., Berggren, P.O., Caicedo, A., 2006. *Proc. Natl. Acad. Sci. U. S. A.* 103 (7), 2334–2339.
- Casasnovas, J., Jo, Y., Rao, X., Xuei, X., Brown, M.E., Kua, K.L., 2019. *J. Endocrinol.* 240 (2), 309–323.
- Castiello, F.R., Heileman, K., Tabrizian, M., 2016. *Lab Chip* 16, 409–431.
- Chen, Ch., Cohrs, Ch., Stertmann, J.M., Bozsak, R., Speier, S., 2017. *Mol. Metabol.* 6 (9), 943–957.
- Chowdhury, A., Satagopam, V.P., Manukyan, L., Artemenko, K.A., Fung, Y.M.E., Schneider, R., Bergquist, J., Bergsten, P., 2013. Signaling in insulin-secreting MIN6 pseudoislets and monolayer cells. *J. Proteome Res.* 12 (12), 5954–5962.
- DeFrondo, R.A., Ferrannini, E., Groop, L., Henry, R.R., Herman, W.H., Holst, J.J., Hu, F.B., Kahn, C.R., Raz, I., Shulman, G.I., Simonson, D.C., Testa, M.A., Weiss, R., 2015. *Nat. Rev. Dis. Prim.* 1, 15019.
- Essaouiba, A., Okitsu, T., Jellali, R., Shinohara, M., Danoy, M., Tauran, Y., Legallais, C., Sakai, Y., Leclerc, E., 2020. *Mol. Cell. Endocrinol.* 514, 11089.
- Guo-Parke, H., McCluskey, J.T., Kelly, C., Hamid, M., McClenaghan, N.H., Flatt, P.R., 2012. *J. Endocrinol.* 214 (3), 257–265.
- Gylfe, E., 2016. *Ups. J. Med. Sci.* 121 (2), 120–132.
- Hassan, S., Sebastian, S., Mahajan, S., Lesha, A., Carpenter, A.M., Liu, X., Xie, X., Livermore, C., Zhang, Y.S., Zarrinpar, A., 2020. *Hepatology* 71 (2), 733–740.
- Henquin, J.C., Nenquin, M., Stiernet, P., Ahren, B., 2006. *55(2):441–451.*
- Hirano, K., Konagaya, S., Turner, A., Noda, Y., Kitamura, S., Kotera, H., Iwata, H., 2017. *Biochem. Biophys. Res. Commun.* 487 (2), 344–350.
- Huh, D., Matthews, B.D., Mammoto, A., Montoya-Zavala, M., Yuan Hsin, H., Ingber, D.E., 2010. *Science* 328 (5986), 1662–1668.
- Jia, D., Dajusta, D., Foty, R.A., 2007. *Dev. Dynam.* 236 (8), 2039–2049.
- Jia, W., Weng, J., Zhu, D., Ji, L., Lu, J., Zhou, Z., Zou, D., Guo, L., Ji, Q., Chen, Li., Chen, Liming, Dou, J., Guo, X., Kuang, H., Li, L., Li, Q., Li, X., Liu, J., Ran, X., Shi, L., Song, G., Xiao, X., Yang, L., Zhao, Z., 2019. *Diabetes. Metab. Res. Rev.* 32 (5), 442–458.
- Jun, Y., Lee, J.S., Choi, S., Yang, J.H., Sander, M., Chung, S., Lee, S.H., 2019. *Sci. Adv.* 5, 11.
- Kahn, S.E., Cooper, M.E., Del Prato, S., 2014. *Lancet* 383 (9922), 1068–1083.
- Katsarou, A., Gudbjörnsdóttir, S., Rawshani, A., Dabelea, D., Bonifacio, E., Anderson, B.J., Jacobsen, L.M., Schatz, D.A., Lernmark, A., 2017. *Nat. Rev. Dis. Prim.* 30 (3), 17016.
- Kim, S.H., Lee, G.H., Park, J.Y., 2013. *Biomed. Eng. Lett.* 3 (131–137).
- Komatsu, H., Gonzalez, N., Salgado, M., Cook, C.A., Li, J., Rawson, J., Omori, K., Tai, Y.-C., Kandeel, F., Mullen, Y., 2020. *Transpl. Int.* 33 (7), 806–818.
- Komatsu, M., Takei, M., Ishii, H., Sato, Y., 2013. *J. Diabetes Investig.* 4 (6), 511–516.
- Korbut, G.S., Mallett, A.G., Ao, Z., Flashner, M., Rajotte, R.V., 2004. *Diabetologia* 47 (10), 1810–1818.
- Lee, S.H., Hong, S.G., Song, J., Cho, B., Han, E.J., Kondapavulur, S., Kim, D., Lee, L.P., 2018. *Adv. Healthc. Mater.* 7 (2), 1701111.
- Liu, W., Kin, T., Ho, S., Dorrell, C., Campbell, S.R., Luo, P., Chen, X., 2019. *EBioMedicine* 50, 306–316.
- Mohammed, J.S., Wang, Y., Harvat, T.A., Oberholzer, J., Eddington, D.T., 2009. *Lab Chip* 9, 97–106.
- Rodeman, K.B., Hatipoglu, B., 2018. *Cleve. Clin. J. Med.* 85 (12), 931–937.
- Röder, P.V., Wu, B., Liu, Y., Han, W., 2016. *Exp. Mol. Med.* 11, e219, 48(3).
- Rodriguez-Diaz, R., Molano, R.D., Weitz, J.R., Abdulreda, M.H., Berman, D.M., Leibiger, B., Leibiger, I.B., Kenyon, N.S., Ricordi, C., Pileggi, A., Caicedo, A., Berggren, P.O., 2018. *Cell Metabol.* 27 (3), 549–558 e4.
- Sokolowska, P., Janikiewicz, J., Jastrzebska, E., Brzozka, Z., Dobrzyn, A., 2020. *Biosens. Bioelectron.* 1 (167), 112451.
- St-Onge, L., Wehr, R., Gruss, P., 1999. *Curr. Opin. Genet. Dev.* 9 (3), 295–300.
- Steiner, D.J., Kim, A., Miller, K., Hara, M., 2010. *Islets* 2 (3), 135–145.
- Ware, M.J., Colbert, K., Keshishian, V., Ho, J., Corr, S.J., Curley, S.A., Godin, B., 2016. *Tissue Eng. C Methods* 22 (4), 312–321.
- Weber, E.J., Lidberg, K.A., Wang, L., Bammler, T.K., MacDonald, J.W., Li, M.J., Redhair, M., Atkins, W.M., Tran, C., Hines, K.M., Herron, J., Xu, L., Monteiro, M.B., Ramm, S., Vaidya, V., Vaara, M., Vaara, T., Himmelfarb, J., Kelly, E.J., 2018. *JCI insight* 3 (24), e123673.
- Wszola, M., Idaszek, J., Berman, A., Kosik, A., Gorski, L., Jozwik, A., Dobrzyn, A., Cudnoch-Jędrzejewska, A., Kaminski, A., Wrzesien, R., Serwanska-Swietek, M., Chmura, A., Kwiatkowski, A., Swieszkowski, W., 2015. *MEDtube Sci.* 3, 25–27.
- Yeo, L.Y., Chang, H.C., Chan, P.P.Y., Friend, J.R., 2011. *Small* 7 (1), 12–48, 3.
- Zheng, Y., Ley, S.H., Hu, F.B., 2018. *Nat. Rev. Endocrinol.* 14 (2), 88–98.
- Zuchowska, A., Jastrzebska, E., Zukowski, K., Chudy, M., Dybko, A., Brzozka, Z., 2017. *Biomicrofluidics* 11 (2), 024110.